JOURNAL OF GUIDANCE, CONTROL, AND DYNAMICS
Vol. 28, No. 5, September–October 2005

Linear Stability Analysis of Electrodynamic Tethers

L. Somenzi* and L. Iess†
University of Rome "La Sapienza," I-00184 Rome, Italy
and
J. Peláez‡
Universidad Politécnica de Madrid, E-28040 Madrid, Spain

It is well known that an electrodynamic tether exhibits dynamic instabilities. A mathematical model of the system under some simplifying assumptions is developed. An inextensible wire with two point end masses in a circular orbit is considered; the conductor is insulated from the ambient plasma. The system attitude dynamics is analyzed within a linear approximation, and the tether lateral oscillations are expanded in normal modes. It is found that the electrodynamic forces cause the coupling of all cable oscillations. The lateral modes acquire frequencies of the same order of magnitude as the frequencies of the librations. At a nonnull inclination, a source of instability is found to be associated to a mechanism of classical resonance between the out-of-plane libration and the electrodynamic forcing terms. Because of their coupling with the librations, the lateral modes are also destabilized, with odd lateral modes more excited than the even ones. The geomagnetic field and the tether current have Fourier spectra rich in frequencies, and this makes the start of instability easier.

Introduction

A CENTRAL issue regarding any electrodynamic tether is its intrinsic instability.[1–9] Over short periods of time the Lorentz forces can dangerously bend the cable and make its librations grow up to a point when the tether flips over and starts tumbling. When this situation occurs, the system loses its deorbiting (or thrusting) capabilities and becomes completely uncontrollable.

In this paper, we carry out a model of an electrodynamic tether, considered as a flexible and inextensible structure. We focus the analysis on its attitude dynamics, with the main goal of identifying the mechanisms responsible for the instability.

This problem has been tackled in previous works with different dynamic and environmental models. Under the assumption of a rigid rod with point end masses (dumbbell model), Ref. 1 shows that the instability source is a nonlinear resonance mechanism that pumps energy into the system. The thread flexibility is included in Refs. 2–4, where very simplified models are adopted to describe the Earth's magnetic field and the wire current. In Ref. 2, the geomagnetic field is modeled as a dipole aligned with the Earth's rotation axis, and the current is assumed to be constant and hence independent of the attitude and orbital position of the tether. In Refs. 3 and 4, a tilted magnetic dipole model and the current modulation coming from the day–night change of the ionospheric density are introduced. Following the example of Ref. 1, we use more realistic models to represent the geomagnetic and ionospheric environment, emphasizing their role in destabilizing the cable. In Refs. 2–4, the system attitude dynamics equations are written in the orbital frame, and the thread oscillations are expanded about the local vertical. In contrast, in this paper we introduce a body-fixed frame, where the attitude dynamics equations are approximated to the first order. In this frame, it is possible to study the tether lateral oscillations as stationary vibrations of a stretched string fixed at both ends, leading to a consistent reduction of the mathematical complexity of the problem. Within the linear approximation, we show some important effects introduced by the electrodynamic forces and identify a mechanism of instability, coming from a classical resonance between the out-of-plane libration and the electrodynamic forces.

The paper is organized as follows. In the next section, the mathematical model of a flexible inextensible tether is developed. The system attitude dynamics equations are then written and approximated to the first order. This is followed by a numerical analysis showing the different behavior of the system in the absence and in the presence of the electrodynamic forces. The mechanism for the onset of the instability is then described. Concluding remarks are offered in the last section.

Tether Model

An electrodynamic tether system (ETS) is made up of a thin conductive wire connected to a satellite. The other thread termination is usually occupied by a ballast, which facilitates the deployment of the cable and helps in stabilizing the system through gravity gradient force. The relative motion at speed $\boldsymbol{v}$ between the satellite and the Earth's magnetic field lines generates an induced potential difference between the two ends of the system equal to

$$\Phi_{\mathrm{ED}} = \int_0^L (\boldsymbol{v} \times \boldsymbol{B}) \cdot \boldsymbol{ds} \tag{1}$$

where L is the tether length, $\boldsymbol{B}$ is the magnetic field, and $\boldsymbol{ds}$ is the differential element of the cable length (pointing toward upper directions). For eastward low Earth orbit (LEO) orbits, a tether deployed upward charges at a positive voltage with respect to the ionosphere at the top end and negatively at the bottom end. If both ends of the system are in electrical contact with the ionospheric plasma, a current I can flow in the wire and an electrodynamic force

$$\boldsymbol{F}_{\mathrm{ED}} = \int_0^L I\boldsymbol{ds} \times \boldsymbol{B} \tag{2}$$

will be exerted on the thread. The electrical contacts can be obtained by means of a passive charge collector placed at the positive termination of the cable and an electron emitter at the negative termination (a hollow cathode or a field emitter array cathode). Equation (2) shows that the electrical current in the wire is the crucial quantity determining the orbital evolution of a conductive tether. The current

Received 27 June 2004; presented as Paper 2003-539 at the AAS/AIAA Astrodynamics Specialists Conference, Big Sky, MT, 3–7 August 2004; accepted for publication 22 December 2004.

*Postdoc, Dipartimento di Ingegneria Aerospaziale ed Astronautica, via Eudossiana 18; somenzi@hermes.diaa.uniroma1.it.

†Associate Professor, Dipartimento di Ingegneria Aerospaziale ed Astronautica, via Eudossiana 18; iess@hermes.diaa.uniroma1.it.

‡Associate Professor, Escuela Tecnica Superior de Ingenieros Aeronáuticos, Plaza Cardenal Cisneros 3; jpelaez@faia.upm.es.

depends, in general, on the characteristics of the electrical contacts between the terminations, the wire itself, and the surrounding ambient plasma. These electrical contacts are usually described by nonlinear current–voltage (I–V) characteristics, which are affected, in turn, by the plasma parameters (namely, density, temperature, and ion composition). Applying the Ohm's law to the equivalent circuit and referring for simplicity to an insulated (unexposed) tether, one may write

$$I = \Phi_{\mathrm{ED}}/R_{\mathrm{tot}}$$

where R_{tot} is the total electric resistance of the circuit given by

$$R_{\mathrm{tot}} = R_w + R_{\mathrm{sh}+} + R_{\mathrm{sh}-} + R_i$$

The breakdown of the total resistance into its components shows the resistance of the wire R_w, the resistance of the ionospheric loop R_i (usually negligible), and the impedances associated with the plasma sheaths at the positive and negative terminations $R_{\mathrm{sh}+}$ and $R_{\mathrm{sh}-}$. The vector $\boldsymbol{F}_{\mathrm{ED}}$ has a component in the opposite direction with respect to the satellite velocity and then acts as a drag force that lowers the orbit (deboost mode). Consequently, electrodynamic tethers can be employed to deorbit LEO objects at the end of their operational life (satellites and rocket upper stages). This application is significant with respect to the problem of the increasing population of debris in near Earth's orbits. If an adequate power supply is available to revert the natural polarity, the current will flow in the opposite direction and a thrust force will be obtained (thrust mode). In this case, the tether acts as a propulsion system with a very high specific impulse. This application has been considered to counteract the atmospheric drag of the International Space Station.

In this paper, a tether model is developed starting from the following simplifying assumptions[10]:

1) The tether is inextensible.

2) The system center of mass coincides with the satellite center of mass.

3) The satellite and the ballast are point masses.

4) The spacecraft moves along an unperturbed circular orbit.

The variations in the cable length caused by the gravity gradient and Lorentz forces are negligible if compared to the total length. (This justifies the first hypothesis.) Thermal expansion of the tether also has small effects. The mass of the main body (from which the tether is deployed) is usually much larger than the remaining masses of the ETS and, consequently, the system c.m. is not far from the main body (second hypothesis). The attitude degrees of freedom of the two end masses of the cable and any orbital perturbation affecting the satellite motion are neglected in this paper (third and fourth hypotheses). The tether is assumed to be electrically insulated from the ambient plasma, and a passive charge collection is provided by a spherical balloon at the anodic termination. In this configuration, the current is constant along the wire and depends on time, due to attitude motions and variations in the ionospheric density. [See Eqs. (1) and (2)].

Let us introduce two right-oriented reference frames (Fig. 1):

1) The first frame is the orbital frame (OF), with origin in the c.m., defined by unit vectors ($\hat{\boldsymbol{r}}$, $\hat{\boldsymbol{v}}$, $\hat{\boldsymbol{h}}$), where $\hat{\boldsymbol{r}}$ is directed from the Earth to the spacecraft and represents the system local vertical, $\hat{\boldsymbol{h}}$ is the orbital angular momentum unit vector, and $\hat{\boldsymbol{v}} = \hat{\boldsymbol{h}} \times \hat{\boldsymbol{r}}$;

2) The second frame is the body-fixed frame (BF), with origin in the c.m., defined by unit vectors ($\hat{\boldsymbol{b}}_1$, $\hat{\boldsymbol{b}}_2$, $\hat{\boldsymbol{b}}_3$), where $\hat{\boldsymbol{b}}_1$ always points to the ballast mass, $\hat{\boldsymbol{b}}_2$ is orthogonal to $\hat{\boldsymbol{b}}_1$ and contained in the orbital plane, and $\hat{\boldsymbol{b}}_3 = \hat{\boldsymbol{b}}_1 \times \hat{\boldsymbol{b}}_2$.

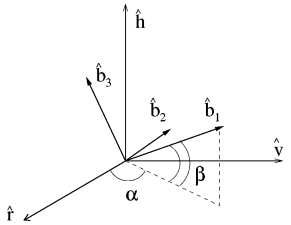

Fig. 1 OF and BF frames.

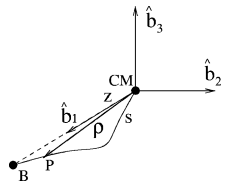

Fig. 2 Tether system in BF; satellite and balloon are located at c.m. and at point B, respectively.

The transformation between the two frames is

$$\begin{bmatrix} \hat{\boldsymbol{r}} \\ \hat{\boldsymbol{v}} \\ \hat{\boldsymbol{h}} \end{bmatrix} = \begin{bmatrix} \cos\alpha\cos\beta & -\sin\alpha & -\cos\alpha\sin\beta \\ \sin\alpha\cos\beta & \cos\alpha & -\sin\alpha\sin\beta \\ \sin\beta & 0 & \cos\beta \end{bmatrix} \begin{bmatrix} \hat{\boldsymbol{b}}_1 \\ \hat{\boldsymbol{b}}_2 \\ \hat{\boldsymbol{b}}_3 \end{bmatrix}$$

where α and β are the in-plane and out-of-plane libration angles.

In the BF frame, the position of a generic tether point P at time t is

$$\boldsymbol{\rho}(s,t) = \rho_1(s,t)\hat{\boldsymbol{b}}_1 + \rho_2(s,t)\hat{\boldsymbol{b}}_2 + \rho_3(s,t)\hat{\boldsymbol{b}}_3$$

where s is the curvilinear coordinate along the tether (Fig. 2). In the dumbbell model, the whole thread lies along $\hat{\boldsymbol{b}}_1$, and, consequently, $\rho_1(s,t) = s$ and $\rho_2(s,t) = \rho_3(s,t) = 0$. Let us write $\rho_1(s,t) = z + u(s,t)$, where $u(s,t)$ is the longitudinal displacement of point P with respect to the tether straight configuration $s = z$. In particular, at $s = L$, we have $\boldsymbol{\rho}(L,t) = \rho_1(L,t)\hat{\boldsymbol{b}}_1 = (L + u(L,t))\hat{\boldsymbol{b}}_1$, with $u(L,t) \le 0$.

If we neglect any tether deployment or retrieval, the system attitude dynamics equations written in the BF reference frame are

$$\lambda[\ddot{\boldsymbol{\rho}} + \dot{\boldsymbol{\Omega}} \times \boldsymbol{\rho} + \boldsymbol{\Omega} \times (\boldsymbol{\Omega} \times \boldsymbol{\rho}) + 2\boldsymbol{\Omega} \times \dot{\boldsymbol{\rho}} - \boldsymbol{G} \cdot \boldsymbol{\rho}]$$

$$= \frac{\partial}{\partial s}\left(T\frac{\partial \boldsymbol{\rho}}{\partial s}\right) + I\frac{\partial \boldsymbol{\rho}}{\partial s} \times \boldsymbol{B} \tag{3}$$

$$\left|\frac{\partial \boldsymbol{\rho}}{\partial s}\right| = 1 \quad \text{(inextensible tether assumption)} \tag{4}$$

where scalar λ is the thread mass per unit length, tensor $\boldsymbol{G} = \omega^2(3\hat{\boldsymbol{r}}\hat{\boldsymbol{r}} - \boldsymbol{1})$ is the first-order gradient of the gravity acceleration ($\boldsymbol{1}$ denoting the unit matrix), and $T(s,t)$ is the cable tension. The vector $\boldsymbol{\Omega}$ represents the angular velocity of the BF reference frame with respect to an inertial frame and can be written as

$$\boldsymbol{\Omega} = \boldsymbol{\omega} + \boldsymbol{\omega}_{\mathrm{rel}}$$

where $\boldsymbol{\omega}$ is the system orbital angular velocity and $\boldsymbol{\omega}_{\mathrm{rel}}$ is the angular velocity of the BF frame with respect to the OF. In Eq. (3), the terms $\boldsymbol{\Omega} \times (\boldsymbol{\Omega} \times \boldsymbol{\rho})$ and $2\boldsymbol{\Omega} \times \dot{\boldsymbol{\rho}}$ are, respectively, the centripetal and the Coriolis accelerations, and $I(\partial\boldsymbol{\rho}/\partial s) \times \boldsymbol{B}$ denotes the electrodynamic force per unit length.

The first boundary condition, to be imposed at $s = L$, is

$$m_b[\ddot{\boldsymbol{\rho}} + \dot{\boldsymbol{\Omega}} \times \boldsymbol{\rho} + \boldsymbol{\Omega} \times (\boldsymbol{\Omega} \times \boldsymbol{\rho}) + 2\boldsymbol{\Omega} \times \dot{\boldsymbol{\rho}} - G \cdot \boldsymbol{\rho}]_{s=L}$$

$$= -T(L,t)\left.\frac{\partial \boldsymbol{\rho}}{\partial s}\right|_{s=L} \tag{5}$$

where m_b is the balloon mass. Notice that the Lorentz force does not appear in Eq. (5). In fact, we can assume that the balloon is equivalent to a tether element of length $\Delta l \sim r_b$ (r_b being the balloon radius), and, consequently, the intensity of the electrodynamic force acting on it is equal to

$$F_b \approx I\,\Delta l\,B$$

Because $r_b \ll L$ and excluding the case of large currents, F_b is much smaller than the remaining terms appearing in Eq. (5) and can, therefore, be neglected.[3] The second boundary condition, to be imposed at $s = 0$, is simply

$$\boldsymbol{\rho}(0,t) = \boldsymbol{0} \tag{6}$$

First-Order Approximation

Without the electrodynamic forces, the stable equilibrium configuration of the system is represented by all of its oscillations equal to zero, that is, $\alpha = \beta = \rho_{2,3} = 0$ and $\rho_1 = s$. (The tether lies along the local vertical.) This configuration corresponds to a steady solution of the attitude dynamics equations. However, when a current flows in the tether, no equilibrium solution is possible due to the presence of the electrodynamic forcing terms. If a centered dipole aligned with the Earth's rotation axis is used to describe the geomagnetic field, the forcing terms become periodic and the governing equations have time-dependent periodic solutions.[2] In such a case, the stability properties of the periodic solutions turn out to be a good measure of the stability properties of the system as a whole. Because we are using a more realistic model to represent the geomagnetic field, no periodic solution can be found for most values of the physical parameters and, consequently, cannot be used as a reference to draw conclusions about the stability properties of the system. A different approach will be adopted in this paper. We will consider only small librations around the local vertical ($\alpha, \beta \ll 1$) and small deviations from the dumbbell configuration ($\rho_{2,3}/L \ll 1$) and will retain only the first-order terms in the equations. This approximation holds as long as the current flowing in the wire is low (about 1 A for a 5 km tether in LEO) and, consequently, the thread is not excited much by the Lorentz forces.

The analysis will be restricted to the realistic case of a thread much lighter than the ballast. Under this hypothesis, the contribution to the tether tension from the wire mass can be neglected. The tension is, therefore, constant along the cable and equal to the value acquired at the ballast end,[11]

$$T \simeq 3\omega^2 m_b L$$

In the remainder of the paper, we use the suffixes s and z to denote the partial derivatives with respect to s and z. If we assume that ρ_{2s} and ρ_{3s} are of the same order as oscillations ρ_2 and ρ_3, scalar u (measuring the longitudinal displacement of a point from the dumbbell configuration) becomes a quantity of the second order (and, therefore, can be neglected) because

$$\left|\frac{\partial \boldsymbol{\rho}}{\partial s}\right| = 1 \Longrightarrow u_s = -\frac{\left(\rho_{2s}^2 + \rho_{3s}^2\right)}{2}$$

Finally, in the linear regime

$$\frac{\mathrm{d}s}{\mathrm{d}z} = \left[(1+u_z)^2 + \rho_{2z}^2 + \rho_{3z}^2\right]^{\frac{1}{2}} \simeq 1 \Longrightarrow s \simeq z$$

We obtain $\boldsymbol{\rho}(L,t) = L\hat{\boldsymbol{b}}_1$, and Eqs. (3), (5), and (6) reduce to the following scalar form along unit vectors $\hat{\boldsymbol{b}}_2$ and $\hat{\boldsymbol{b}}_3$:

$$\lambda\left\{\ddot{\rho}_2 + z[\ddot{\alpha}(t) + 3\omega^2\alpha(t)]\right\} = T\rho_{2zz} + I[\rho_{3z} + \beta(t)]B_r(t) - IB_h(t) \tag{7}$$

$$\lambda\left\{\ddot{\rho}_3 + \omega^2\rho_3 + z[\ddot{\beta}(t) + 4\omega^2\beta(t)]\right\} = T\rho_{3zz} - I[\rho_{2z} + \alpha(t)]B_r(t) + IB_v(t) \tag{8}$$

$$\ddot{\alpha}(t) + 3\omega^2\alpha(t) = -T\rho_{2z}(L,t)/(m_b L) \tag{9}$$

$$\ddot{\beta}(t) + 4\omega^2\beta(t) = -T\rho_{3z}(L,t)/(m_b L) \tag{10}$$

$$\rho_2(0,t) = \rho_3(0,t) = 0 \tag{11}$$

$$\rho_2(L,t) = \rho_3(L,t) = 0 \tag{12}$$

B_r, B_v, and B_h are the components of the magnetic field expressed in the orbital reference frame:

$$\boldsymbol{B} = B_r\hat{\boldsymbol{r}} + B_v\hat{\boldsymbol{v}} + B_h\hat{\boldsymbol{h}}$$

Not surprisingly, the librations and the lateral modes are coupled through the tension terms [Eqs. (9) and (10)], the inertial terms ($\ddot{\alpha}$, $\ddot{\beta} + \omega^2\beta$), and the terms due to the gradient of the gravity acceleration ($3\omega^2\alpha$, $3\omega^2\beta$) [Eqs. (7) and (8)]. The electrodynamic forces introduce source forcing terms and a coupling of the oscillations pertaining to orthogonal planes: α with β and ρ_2 with ρ_3.

The attitude dynamics of the dumbbell model is recovered by carrying out the following steps:

1) Multiply both members of Eqs. (7) and (8) by the quantity $z\,dz$ and integrate them in the interval $z = (0, L)$.

2) Multiply both members of Eqs. (9) and (10) by the quantity $m_b L^2$, which represents in the dumbbell model the moment of inertia of the ballast mass with respect to the c.m.

3) Sum Eqs. (7) and (9) and Eqs. (8) and (10).

4) Turn off the lateral modes $\rho_{2,3}$ by putting them and their derivatives equal to zero for all of the values of s and t.

One then recovers the linear approximation to the attitude dynamics equations of the dumbbell model:

$$\ddot{\alpha}(t) + 3\omega^2\alpha(t) = AB_r(t)\beta(t) - AB_h(t)$$

$$\ddot{\beta}(t) + 4\omega^2\beta(t) = -AB_r(t)\alpha(t) + AB_v(t)$$

$$A = Id_{\mathrm{med}}L/J$$

Here $d_{\mathrm{med}} = L/2$ is the distance between the c.m. and tether geometrical center, and $J = m_b L^2 + m_t L^2/3$ is the moment of inertia of the system with respect to the c.m. (m_t being the tether mass). These equations coincide with the linearized version of Eqs. (11) of Ref. 1 and with Eqs. (6) and (7) of Ref. 5.

In a dimensionless form, that is, when the temporal derivative is calculated with respect to the true anomaly $\tau = \omega t$ and all of the lengths are divided by L ($z \to z/L$ and $\rho_i \to \rho_i/L$), Eqs. (7–12) become

$$\ddot{\rho}_2 + z(\ddot{\alpha} + 3\alpha) = p\rho_{2zz} + \epsilon_r(\tau)(\rho_{3z} + \beta) - \epsilon_h(\tau)$$

$$\ddot{\rho}_3 + \rho_3 + z(\ddot{\beta} + 4\beta) = p\rho_{3zz} - \epsilon_r(\tau)(\rho_{2z} + \alpha) + \epsilon_v(\tau)$$

$$\ddot{\alpha} + 3\alpha = -3\rho_{2z}(1,\tau)$$

$$\ddot{\beta} + 4\beta = -3\rho_{3z}(1,\tau)$$

$$\rho_2(0,\tau) = \rho_3(0,\tau) = 0$$

$$\rho_2(1,\tau) = \rho_3(1,\tau) = 0 \tag{13}$$

where $p = 3/\mu$, $\mu = m_t/m_b$, $\epsilon_r(\tau) = IB_r(\tau)/(m_t\omega^2)$, $\epsilon_v(\tau) = IB_v(\tau)/(m_t\omega^2)$, and $\epsilon_h(\tau) = IB_h(\tau)/(m_t\omega^2)$.

In the linear approximation, the cable terminations are fixed in a BF frame because they lie by definition along $\hat{\boldsymbol{b}}_1$, and the oscillations along this axis, represented by scalar u, are of higher order. Therefore, the tether lateral oscillations can be studied as stationary vibrations of a stretched string with both ends fixed and can be expanded in a Fourier series of orthogonal trigonometric functions in the interval $z = (0, 1)$:

$$\rho_2(z,\tau) = \sum_{n=1}^{\infty} x_n(\tau)\sin(k_n z), \qquad \rho_3(z,\tau) = \sum_{n=1}^{\infty} y_n(\tau)\sin(k_n z)$$

$$k_n = n\pi$$

Let us write the functions involved in system (13) in series of $\sin(k_n z)$,

$$1 = \frac{4}{\pi}\sum_{n\,\mathrm{odd}}\frac{1}{n}\sin(k_n z)$$

$$z = \frac{2}{\pi}\sum_{n=1}^{\infty}\frac{(-1)^{(n+1)}}{n}\sin(k_n z)$$

$$\cos(k_l z) = \sum_{n=1}^{\infty} I_{ln}\sin(k_n z)$$

where

$$I_{ln} = 0$$

if l and n have the same parity, and where

$$I_{ln} = (4/\pi)[n/(n^2 - l^2)]$$

if l and n have the opposite parity.

The system of partial differential equations (13) can be reduced to one of ordinary differential equations for the functions α, β, x_n, and y_n by exploiting the orthogonality properties of $\sin(k_n z)$:

$$\text{odd } n \begin{cases} \ddot{x}_n + pk_n^2 x_n + \dfrac{2}{n\pi}(\ddot{\alpha} + 3\alpha) \\ \quad = \epsilon_r(\tau) \displaystyle\sum_{l\,\text{even}} I_{ln} k_l y_l + \frac{4}{n\pi}[\epsilon_r(\tau)\beta - \epsilon_h(\tau)] \\ \ddot{y}_n + \left(1 + pk_n^2\right) y_n + \dfrac{2}{n\pi}(\ddot{\beta} + 4\beta) \\ \quad = -\epsilon_r(\tau) \displaystyle\sum_{l\,\text{even}} I_{ln} k_l x_l - \frac{4}{n\pi}[\epsilon_r(\tau)\alpha - \epsilon_v(\tau)] \end{cases} \quad (14)$$

$$\text{even } n \begin{cases} \ddot{x}_n + pk_n^2 x_n - \dfrac{2}{n\pi}(\ddot{\alpha} + 3\alpha) = \epsilon_r(\tau) \displaystyle\sum_{l\,\text{odd}} I_{ln} k_l y_l \\ \ddot{y}_n + \left(1 + pk_n^2\right) y_n - \dfrac{2}{n\pi}(\ddot{\beta} + 4\beta) = -\epsilon_r(\tau) \displaystyle\sum_{l\,\text{odd}} I_{ln} k_l x_l \end{cases} \quad (15)$$

$$\ddot{\alpha} + 3\alpha = 3 \sum_{n=1}^{\infty} (-1)^{n+1} k_n x_n \quad (16)$$

$$\ddot{\beta} + 4\beta = 3 \sum_{n=1}^{\infty} (-1)^{n+1} k_n y_n \quad (17)$$

Note that the forcing terms $4[\epsilon_r(\tau)\beta - \epsilon_h(\tau)]/n\pi$ and $4[-\epsilon_r(\tau)\alpha + \epsilon_v(\tau)]/n\pi$ of system (14) do not appear for the even modes. These terms, being independent of the spatial coordinate, are associated to a force uniform along the tether and, therefore, cannot excite the even lateral modes that have a node at the middle point of the system.

Numerical Results

We have applied the decomposition (14–17) to the case of a typical tether system for deorbiting applications (Table 1). The International Geomagnetic Reference Field and the International Reference Ionosphere have been included in the numerical codes, and average levels of solar activity have been considered (150 flux units at 10.7 cm). To obtain a first indication about the mode coupling and a qualitative understanding of the system dynamics, we truncate the system (14–17) to $n = 2$:

$$\ddot{\alpha} + 3\alpha = 3(k_1 x_1 - k_2 x_2) \quad (18)$$

$$\ddot{\beta} + 4\beta = 3(k_1 y_1 - k_2 y_2) \quad (19)$$

Table 1 ETS parameters

Quantity	Element	Symbol	Value
Length	Tether	L	5 km
Density	Tether	ϱ	2.7 g/cm^3 (aluminum)
Radius	Tether	r_w	0.4 mm
Mass	Tether	m_t	7 kg
Mass	Satellite	m_s	500 kg
Mass	Collector	m_b	28 kg
Radius	Collector	r_b	5 m

$$\ddot{x}_1 + pk_1^2 x_1 + 2(\ddot{\alpha} + 3\alpha)/\pi = \epsilon_r I_{21} k_2 y_2 + 4(\epsilon_r \beta - \epsilon_h)/\pi \quad (20)$$

$$\ddot{y}_1 + \left(pk_1^2 + 1\right) y_1 + 2(\ddot{\beta} + 4\beta)/\pi = -\epsilon_r I_{21} k_2 x_2 - 4(\epsilon_r \alpha - \epsilon_v)/\pi \quad (21)$$

$$\ddot{x}_2 + pk_2^2 x_2 - (\ddot{\alpha} + 3\alpha)/\pi = \epsilon_r I_{12} k_1 y_1 \quad (22)$$

$$\ddot{y}_2 + \left(pk_2^2 + 1\right) y_2 - (\ddot{\beta} + 4\beta)/\pi = -\epsilon_r I_{12} k_1 x_1 \quad (23)$$

With the system parameters in Table 1, Eqs. (18–23) reduce to

$$\ddot{\alpha} + 3\alpha = 3\pi(x_1 - 2x_2) \quad (24)$$

$$\ddot{\beta} + 4\beta = 3\pi(y_1 - 2y_2) \quad (25)$$

$$\ddot{x}_1 + 124.4x_1 - 12x_2 = -8\epsilon_r y_2/3 + 4(\epsilon_r \beta - \epsilon_h)/\pi \quad (26)$$

$$\ddot{y}_1 + 125.4y_1 - 12y_2 = 8\epsilon_r x_2/3 - 4(\epsilon_r \alpha - \epsilon_v)/\pi \quad (27)$$

$$\ddot{x}_2 + 479.7x_2 - 3x_1 = 8\epsilon_r y_1/3 \quad (28)$$

$$\ddot{y}_2 + 480.7y_2 - 3y_1 = -8\epsilon_r x_1/3 \quad (29)$$

The numerical analysis was performed for the following two cases: 1) a null tether current along the orbit, with initial conditions corresponding to a tether close to the local vertical and 2) constant current along the orbit, with initial conditions corresponding to a vertical tether ($\alpha = \beta = x_1 = y_1 = x_2 = y_2 = 0$).

Case 1

In the absence of Lorentz forces, Eqs. (24–29) become

$$\ddot{\alpha} + 3\alpha = 3\pi(x_1 - 2x_2) \quad (30)$$

$$\ddot{\beta} + 4\beta = 3\pi(y_1 - 2y_2) \quad (31)$$

$$\ddot{x}_1 + 124.4x_1 - 12x_2 = 0 \quad (32)$$

$$\ddot{y}_1 + 125.4y_1 - 12y_2 = 0 \quad (33)$$

$$\ddot{x}_2 + 479.7x_2 - 3x_1 = 0 \quad (34)$$

$$\ddot{y}_2 + 480.7y_2 - 3y_1 = 0 \quad (35)$$

Not surprisingly, the dynamics of α, x_1, and x_2 are uncoupled from the dynamics of β, y_1, and y_2 (a consequence of the linear approximation). The analytical solution of system (30–35) shows that the lateral modes have much higher frequencies than the libration modes ($\sqrt{3}\omega$ for α, 2ω for β, $\simeq \sqrt{(124.4)}\omega$ for x_1, $\simeq \sqrt{(125.4)}\omega$ for y_1, $\simeq \sqrt{(479.7)}\omega$ for x_2, and $\simeq \sqrt{(480.7)}\omega$ for y_2). One can, therefore, average Eqs. (30) and (31) over times of the order of the period of the high-frequency oscillations, with the result that librations and lateral modes become uncoupled:

$$\ddot{\alpha} + 3\alpha \simeq 0 \quad (36)$$

$$\ddot{\beta} + 4\beta \simeq 0 \quad (37)$$

$$\ddot{x}_1 + 124.4x_1 - 12x_2 = 0 \quad (38)$$

$$\ddot{y}_1 + 125.4y_1 - 12y_2 = 0 \quad (39)$$

$$\ddot{x}_2 + 479.7x_2 - 3x_1 = 0 \quad (40)$$

$$\ddot{y}_2 + 480.7y_2 - 3y_1 = 0 \quad (41)$$

Case 2

The current is kept to a constant level $I = 1$ A along the orbit at 600-km altitude and inclinations $i = 0$ deg (case 2a) and $i = 55$ deg (case 2b).

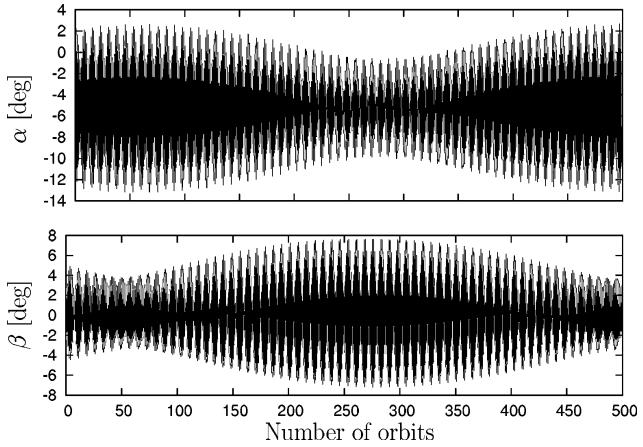

Fig. 3 System librations at 600-km altitude and inclination $i = 0$ deg, for constant current $I = 1$ A.

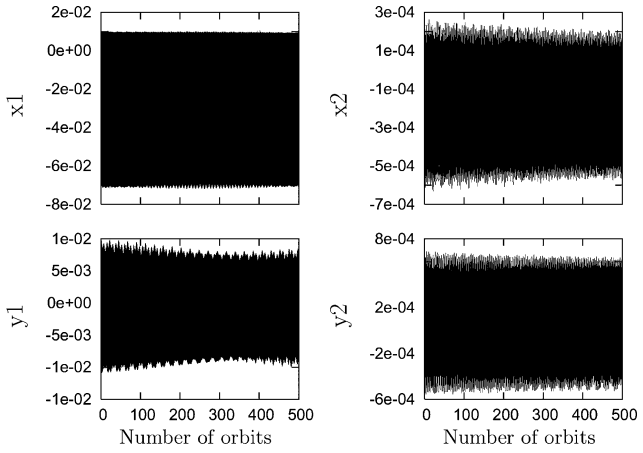

Fig. 4 Normal lateral modes $l = 1$ and $l = 2$ of tether, associated with librations of Fig. 3.

Case 2a ($I = 1$ A, $i = 0$ deg)

Figures 3 and 4 show that the thread oscillations do not grow in 500 orbits (about one month). This stability can be attributed to the fact that at a null inclination the frequencies of the forcing terms (due to the Earth's magnetic field) are decreased by the amount $l\omega_\oplus$, where l is the degree of the harmonic (for instance, $l = 1$ identifying the dipole) and $\omega_\oplus$ is the terrestrial spin frequency ($\omega_\oplus \simeq 0.07\omega$ at 600-km altitude, Fig. 5). This small shift, a consequence of the Earth and magnetic field lines' rotation, is enough to prevent the occurrence of any classical resonance between the out-of-plane libration angle and the electrodynamic forcing terms.

The Fourier spectra of the lateral modes exhibit an interesting behavior (Figs. 6 and 7). Because of the source and coupling forcing terms, the lateral modes take on frequencies of the same order of magnitude as those of the librations. Thus, the presence of the Lorentz forces imposes a common temporal scale that strongly binds together all of the modes. The dynamics of the lateral modes is no longer uncoupled from the dynamics of the librations, as it was found in the absence of current (case 1).

Case 2b ($I = 1$ A, $i = 55$ deg)

A finite inclination changes completely the behavior of the system. The most striking effect is a linear growth of the out-of-plane librations (Fig. 8). (To show this amplification better, the simulation has been extended outside the range of applicability of the linear regime, up to angles $\beta \simeq 45$ deg.) This instability is caused by the occurrence of a classical resonance between angle β and the forcing electrodynamic terms. Indeed, at inclined orbits, the quadrupole harmonic of the geomagnetic field leads to forcing terms at a frequency 2ω (Fig. 9), which is the natural frequency of β [Eq. (25)]. The main

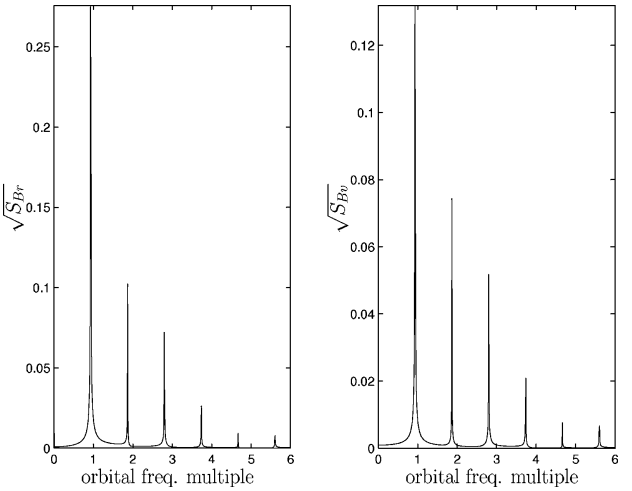

Fig. 5 Spectra of in-plane orbital components of Earth's magnetic field at 600-km altitude and 0-deg inclination; spectra are in arbitrary units, and only relative amplitudes have physical meaning.

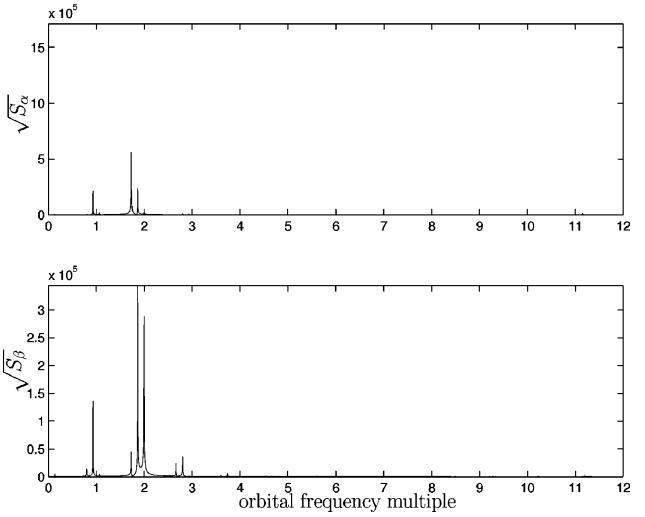

Fig. 6 Spectra of librations corresponding to Fig. 3; spectra are in arbitrary units, and only relative amplitudes have physical meaning.

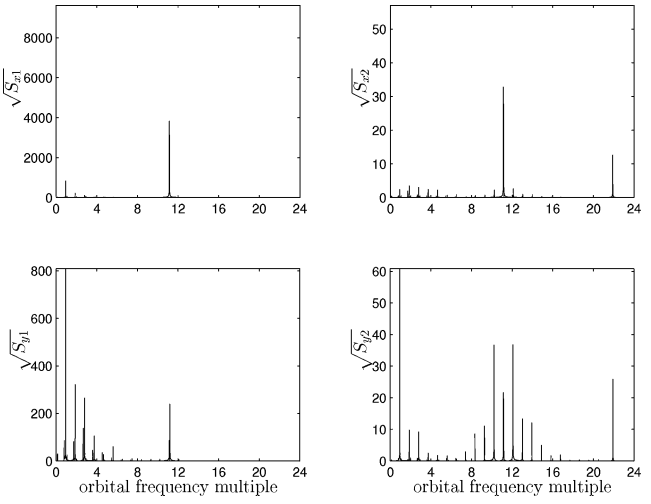

Fig. 7 Spectra of normal lateral modes corresponding to Fig. 4; spectra are in arbitrary units, and only relative amplitudes have physical meaning.

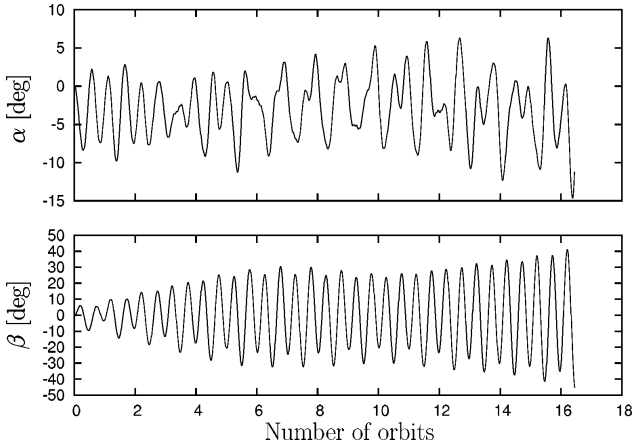

Fig. 8 System librations at 600-km altitude and inclination $i = 55$ deg, for constant current $I = 1$ A along orbit.

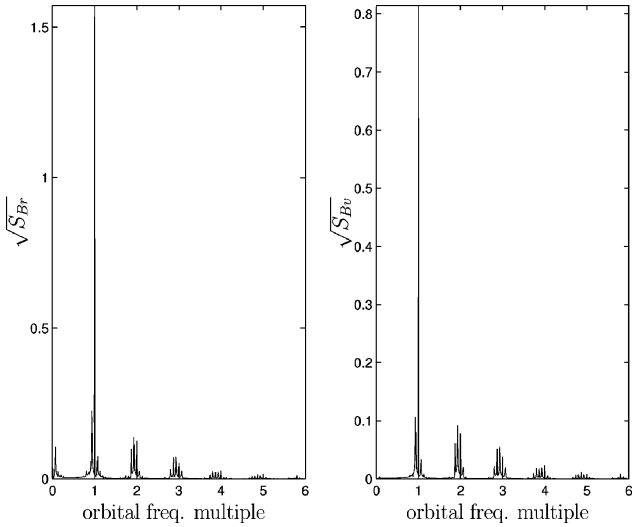

Fig. 9 Spectra of in-plane orbital components of Earth's magnetic field at 600-km altitude and 55-deg inclination; spectra are in arbitrary units, and only relative amplitudes have physical meaning.

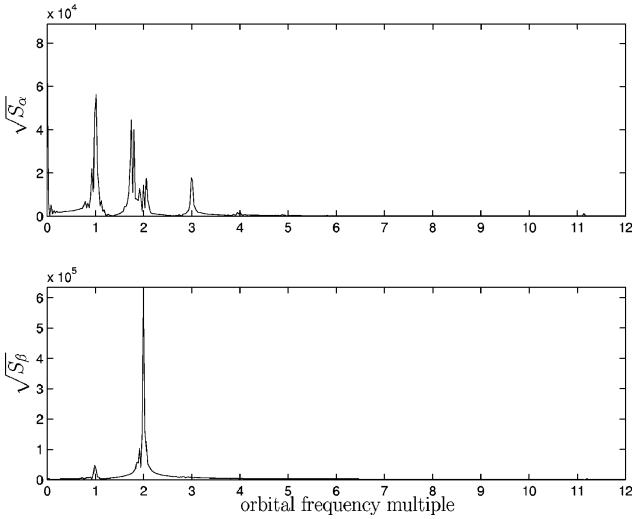

Fig. 10 Spectra of librations corresponding to Fig. 8; spectra are in arbitrary units, and only relative amplitudes have physical meaning.

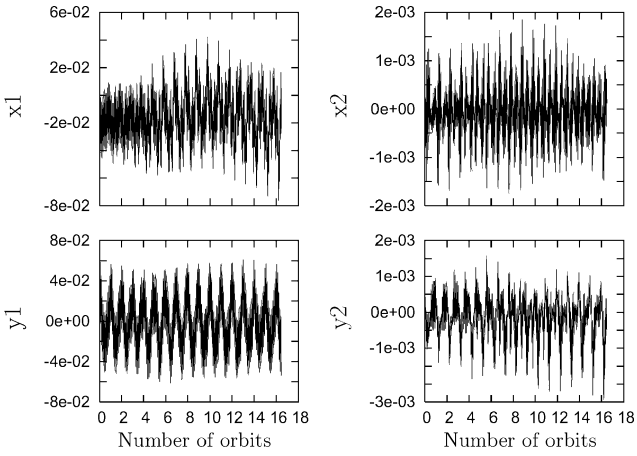

Fig. 11 Normal lateral modes $l = 1$ and $l = 2$ of tether, associated with librations of Fig. 8.

contribution to this instability comes from the source term $4\epsilon_v/\pi$ of Eq. (27), which excites the lateral mode y_1 at a frequency 2ω. As a consequence, β is in classical resonance with the term $3\pi y_1$ of Eq. (25) and begins to grow in amplitude. Because of the strong coupling between the oscillations, the instability of the out-of-plane libration is also transmitted to the other modes. For example, the coupling term $4\epsilon_r\beta/\pi$ of Eq. (26) induces the growth of x_1, which excites y_2 through the term $-8\epsilon_r x_1/3$ of Eq. (29). A further resonance is activated by $-4\epsilon_r\alpha/\pi$ [Eq. (27)] that has a frequency equal to 2ω because both ϵ_r (due to the dipole harmonic of the magnetic field) and angle α (Fig. 10) also possess frequency ω. However, as long as the amplitude of the in-plane angle remains small, this coupling term is approximately one order of magnitude smaller than the source term $4\epsilon_v/\pi$, and the resulting instability is much slower to develop.

The second lateral modes x_2 and y_2 are about one order of magnitude smaller in amplitude than the first modes (Fig. 11). Those modes are indeed excited by the Lorentz forces only through the coupling terms $8\epsilon_r y_1/3$ and $-8\epsilon_r x_1/3$ [Eqs. (28) and (29)]. As long as x_1 and y_1 remain small, these coupling terms are smaller than the source terms $-4\epsilon_h/\pi$ and $4\epsilon_v/\pi$ that force x_1 and y_1 [Eqs. (26) and (27)] and, therefore, cannot efficiently amplify x_2 and y_2. Generally speaking, this consideration applies to all of the even lateral modes. The nth even in-plane mode is coupled to all of the odd out-of-plane modes, and the nth even out-of-plane mode is coupled to all of the odd in-plane modes [Eqs. (15)]. This implies that both equations are free from coupling terms in near resonance with the proper frequency of the corresponding oscillator,[3] and, hence, the even modes are much more difficult to excite than the odd ones. For this reason, we expect that the modes x_{2n+1} and y_{2n+1} are at least of the same order of magnitude as the modes x_{2n} and y_{2n}, whereas they are smaller than the modes x_{2n-1} and y_{2n-1} due to a linear decrease with the index n of the source forcing terms [Eqs. (14)].

The density of the terrestrial ionosphere is extremely variable along the orbit and has a Fourier spectrum rich in frequencies (Fig. 12). If we let the current vary along the orbit instead of setting it to a constant level, new resonances will take place, and the system will become more unstable. To give an example, at a nonnull orbital inclination the harmonic term of the current at frequency ω and the dipole magnetic field give rise to a further classical resonance between angle β and the source term $4\epsilon_v/\pi$. Also, the ionospheric density (and, consequently, the tether current) has nonnegligible harmonics up to 5ω–6ω at inclined orbits. It follows that the forcing terms acquire frequencies close to the natural frequencies of the lateral modes, leading to a strong excitation. The dynamics of the lateral modes when the tether current is determined by the electrical characteristics of the system (in particular, the current–voltage characteristics of the terminations) is shown in Fig. 13 for a 600-km altitude, 55-deg inclination orbit. The average value of the current is about 1 A. The amplitudes of the lateral modes are much more amplified than when the current was kept to 1 A along the orbit at the same inclination (Fig. 11). The first normal modes reach a value of 0.2, corresponding to a deviation of $0.2L = 1$ km.

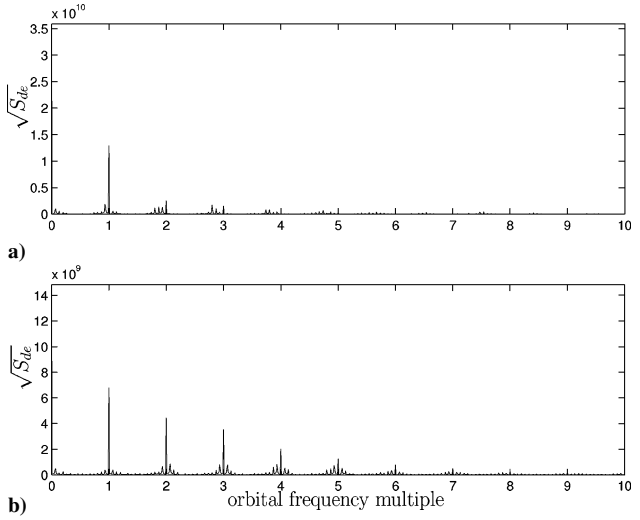

Fig. 12 Spectra of Earth's ionospheric density at 600-km altitude and inclinations a) $i = 0$ deg and b) $i = 55$ deg; spectra are in arbitrary units, and only relative amplitudes have physical meaning.

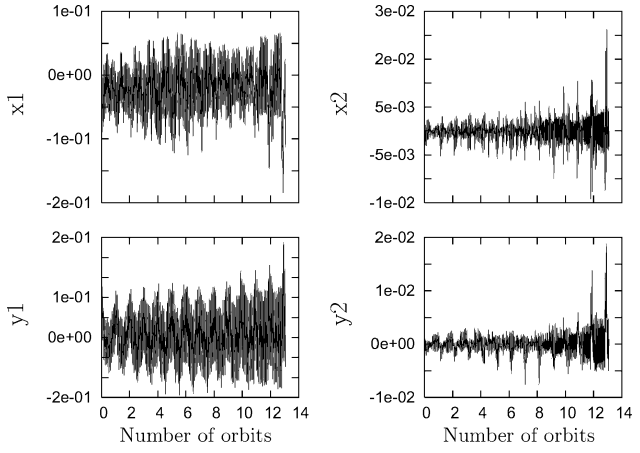

Fig. 13 Normal lateral modes $l = 1$ and $l = 2$ at 600-km altitude and inclination $i = 55$ deg.

Conclusions

The attitude dynamics of an inextensible electrodynamic tether has been analyzed in a first-order approximation. The thread has been considered insulated, and simplifying assumptions have been introduced to reduce the mathematical complexity, namely, the c.m. of the system is located at the satellite; the two terminations of the cable are point masses; and the system c.m. is in a circular orbit. Only the dynamics equations of the librations and of the first two lateral modes, in-plane and out-of-plane, have been included in the numerical analysis.

We found that a source of instability stems from classical resonances occurring at inclined orbits between the out-of-plane libration and the electrodynamic forcing terms. Because of the coupling between all modes, this instability affects the lateral modes too. We have singled out the destabilizing effect of the quadrupole harmonic of the geomagnetic field at a nonnull inclination both at constant and free current levels. In the latter case (when the current is determined by the impedances of each circuit element) the wire becomes more unstable. Indeed, further resonances occur, and the electrodynamic forcing terms acquire frequencies closer to the natural frequencies of the lateral modes, leading to a stronger excitation. The even modes are found to be excited only by coupling terms having frequencies very different from their natural frequencies. Therefore, their amplitude does not grow much.

Note that the system attitude dynamics equations are highly nonlinear. Hence, the linear analysis performed in this paper is far from being exhaustive. The nonlinearity becomes crucial at larger oscillations and must be included to obtain more reliable conclusions about the instability mechanisms.

We have shown that the coupling effect of the electrodynamic forces prevents us from separating the dynamics equations of the librations from those of the lateral modes. Moreover, the electrodynamic forcing terms impose a unique timescale in the system dynamics that reinforces the coupling effects between the different modes. These characteristics should also appear in any analysis where nonlinear effects are considered.

An ETS, due to its intrinsic instability, is useless if it is not properly controlled. The high number of variables to be controlled (the tether modes of oscillation) and their strong coupling increase the complexity of the problem. At the moment the control of an ETS represents a challenging problem that still needs a fully reliable solution.

References

[1]Corsi, J., and Iess, L., "Stability and Control of Electrodynamic Tethers for De-orbiting Applications," *Acta Astronautica*, Vol. 48, No. 5-12, 2001, pp. 491–501.

[2]Ruiz, M., López-Rebollal, O., Lorenzini, E. C., and Peláez, J., "Modal Analysis of the Stability of Periodic Solutions in Electrodynamic Tethers," *Advances in the Astronautical Sciences*, Vol. 109, 2002, pp. 1553–1570.

[3]Dobrowolny, M., "Linear Stability of Electrodynamic Tethers," *Il Nuovo Cimento*, Vol. 25 C, No. 4, 2002, pp. 369–391.

[4]Dobrowolny, M., "Lateral Oscillations of an Electrodynamic Tether," *Journal of Astronautical Sciences*, Vol. 50, No. 2, 2002, pp. 125–147.

[5]Peláez, J., Lorenzini, E. C., López-Rebollal, O., and Ruiz, M., "A New Kind of Dynamic Instability in Electrodynamic Tethers," *Journal of Astronautical Sciences*, Vol. 48, No. 4, 2000, pp. 449–476.

[6]Peláez, J., López-Rebollal, O., Ruiz, M., and Lorenzini, E. C., "Damping in Rigid Electrodynamic Tethers on Inclined Orbits," American Astronautical Society, Paper AAS01-190, Feb. 2001.

[7]Peláez, J., Ruiz, M., López-Rebollal, O., Lorenzini, E. C., and Cosmo, M. L., "A Two-Bar Model for the Dynamics and Stability of Electrodynamic Tethers," *Journal of Guidance, Control, and Dynamics*, Vol. 25, No. 6, 2002, pp. 1125–1135.

[8]Peláez, J., and Lorenzini, E. C., "Libration Control of Electrodynamic Tethers in Inclined Orbits," American Astronautical Society, Paper AAS03-214, Feb. 2003.

[9]Beletsky, V. V., and Levin, E. M., "Dynamics of Space Tether Systems," *Advances in the Astronautical Sciences*, Vol. 83, No. 2, 1992, pp. 189–201.

[10]Bergamaschi, S., and Catinaccio, A., "Further Developments in the Harmonic Analysis of TTS-1," *Journal of Astronautical Sciences*, Vol. 40, No. 2, 1992, pp. 189–201.

[11]Graziani, F., Sgubini, S., and Agneni, A., "Disturbance Propagation in Orbiting Tethers," *Tethers in Space, Advances in the Astronautical Sciences*, Vol. 62, 1986, pp. 301–315.